How to cite: *Angew. Chem. Int. Ed.* **2024**, *63*, e202310623
doi.org/10.1002/anie.202310623

Electrocatalysis

Active Sites of Cobalt Phthalocyanine in Electrocatalytic CO_2 Reduction to Methanol

Conor L. Rooney[+], Mason Lyons[+], Yueshen Wu, Gongfang Hu, Maoyu Wang, Chungseok Choi, Yuanzuo Gao, Chun-Wai Chang, Gary W. Brudvig, Zhenxing Feng, and Hailiang Wang**

Abstract: Many metal coordination compounds catalyze CO_2 electroreduction to CO, but cobalt phthalocyanine hybridized with conductive carbon such as carbon nanotubes is currently the only one that can generate methanol. The underlying structure–reactivity correlation and reaction mechanism desperately demand elucidation. Here we report the first in situ X-ray absorption spectroscopy characterization, combined with ex situ spectroscopic and electrocatalytic measurements, to study CoPc-catalyzed CO_2 reduction to methanol. Molecular dispersion of CoPc on CNT surfaces, as evidenced by the observed electronic interaction between the two, is crucial to fast electron transfer to the active sites and multi-electron CO_2 reduction. CO, the key intermediate in the CO_2-to-methanol pathway, is found to be labile on the active site, which necessitates a high local concentration in the microenvironment to compete with CO_2 for active sites and promote methanol production. A comparison of the electrocatalytic performance of structurally related porphyrins indicates that the bridging aza-N atoms of the Pc macrocycle are critical components of the CoPc active site that produces methanol. In situ X-ray absorption spectroscopy identifies the active site as Co(I) and supports an increasingly non-centrosymmetric Co coordination environment at negative applied potential, likely due to the formation of a Co–CO adduct during the catalysis.

[*] C. L. Rooney,[+] Y. Wu, G. Hu, C. Choi, Y. Gao, G. W. Brudvig, H. Wang
Department of Chemistry, Yale University, New Haven, CT, 06520 (USA)
E-mail: hailiang.wang@yale.edu

C. L. Rooney,[+] Y. Wu, G. Hu, C. Choi, Y. Gao, G. W. Brudvig, H. Wang
Energy Sciences Institute, Yale University, West Haven, CT, 06516 (USA)

M. Lyons,[+] M. Wang, C.-W. Chang, Z. Feng
School of Chemical, Biological, and Environmental Engineering, Oregon State University, Corvallis, OR, 97331 (USA)
E-mail: zhenxing.feng@oregonstate.edu

[+] These authors contributed equally to this work.

Cobalt phthalocyanine (CoPc) is one of the most attractive electrocatalysts for CO_2 reduction.[1] Nearly 40 years ago, Lewis et al. discovered that CoPc deposited on carbon electrodes could reduce CO_2 to CO in aqueous electrolyte.[2] Since then, various heterogeneous CoPc electrocatalysts have been reported, including those where the molecule is supported on carbon nanomaterials,[3] encapsulated in polymers,[4] or built into metal–organic frameworks.[5] Nearly all these reported catalysts demonstrate high selectivity for CO, with some achieving $>95\,\%$ Faradaic efficiency (FE) and over 100 mA/cm^2 partial current density for CO (j_{CO}) with stability for tens of hours.[3c,d] In addition to the reports of selective CO production, an early work found that CoPc catalyzed CO_2 electroreduction to methanol (MeOH),[6] although the partial current and FE were very low. We recently discovered that CoPc noncovalently anchored on multiwalled carbon nanotubes (CoPc/CNT) is highly active for electrochemical CO_2 reduction to MeOH.[7] This was the first report of a molecular catalyst with appreciable activity for MeOH production from CO_2, and the catalyst yields an optimal FE_{MeOH} of 44 % and j_{MeOH} of 10.6 mA/cm^2 at −0.94 V vs the reversible hydrogen electrode (RHE). The catalytic onset occurs at potentials more cathodic than the CO-selective range and MeOH is always produced concomitantly with CO.[7–8] Recent studies demonstrate the robustness of this reaction using slightly modified versions of the catalyst: Ye et al. achieve j_{MeOH} up to 66.8 mA/cm^2 from CO_2 reduction catalyzed by CoPc on single-walled CNTs in a flow-cell reactor,[9] while we report highly selective CO electroreduction to MeOH up to 84 % FE catalyzed by cobalt β-tetraamino-phthalocyanine on CNTs (CoPc–NH_2/CNT).[10] This novel catalytic activity has opened doors to new research directions, such as electrocatalytic C–N coupling that takes advantage of electrophilic intermediates in CO_2 reduction to MeOH to synthesize organonitrogen compounds,[8b,c] as well as photoelectrochemical CO_2-to-MeOH conversion utilizing CoPc integrated with semiconducting silicon.[8d]

Despite the progress made towards developing the unique reactivity of CoPc catalyzing CO_2 electroreduction to MeOH, there remain several key questions regarding the active site and catalytic mechanism of the reaction yet to be answered. Firstly, what is the role of the carbon support in the catalysis? Thus far, all MeOH-producing CoPc electrocatalysts are molecularly dispersed on graphitic carbon

substrates.[7–,8d] Regarding the molecular structure of the catalyst, what motifs are critical to MeOH production and can similar molecules catalyze the reaction? Other Co–N_4 catalysts, such as cobalt porphyrins,[11] corroles,[12] and single-atom catalysts[13] have been reported to produce CO but not MeOH. The catalytic mechanism of the reaction is also uncertain: what are the key intermediates in the CO_2-to-MeOH pathway and do they remain bound to the active site throughout the reaction? Initial work suggests CO is an intermediate, but this fails to explain why MeOH is produced only when there is also a high rate of CO production.[7–8,14] Lastly, what is the oxidation state and coordination environment of Co in the active catalyst? Prior studies have produced contradictory results with some suggesting Co(II)[15] with a doubly reduced ligand and others a Co(I)[16] with a singly reduced ligand active site. Answering these questions is critical to advancing our understanding of electrocatalytic CO_2 reduction chemistry and to developing this CO_2-to-MeOH system toward practical application. Prior spectroscopic and mechanistic studies of CoPc electrocatalysts have been performed on CO_2-to-CO active systems,[16a,17] or very recently a CO-to-MeOH system;[18] however, there are still no prior in situ spectroscopy studies of CoPc operating at CO_2-to-MeOH conditions. Probing the molecular environment at the MeOH-formation active site is needed to help us understand the catalytic pathway.

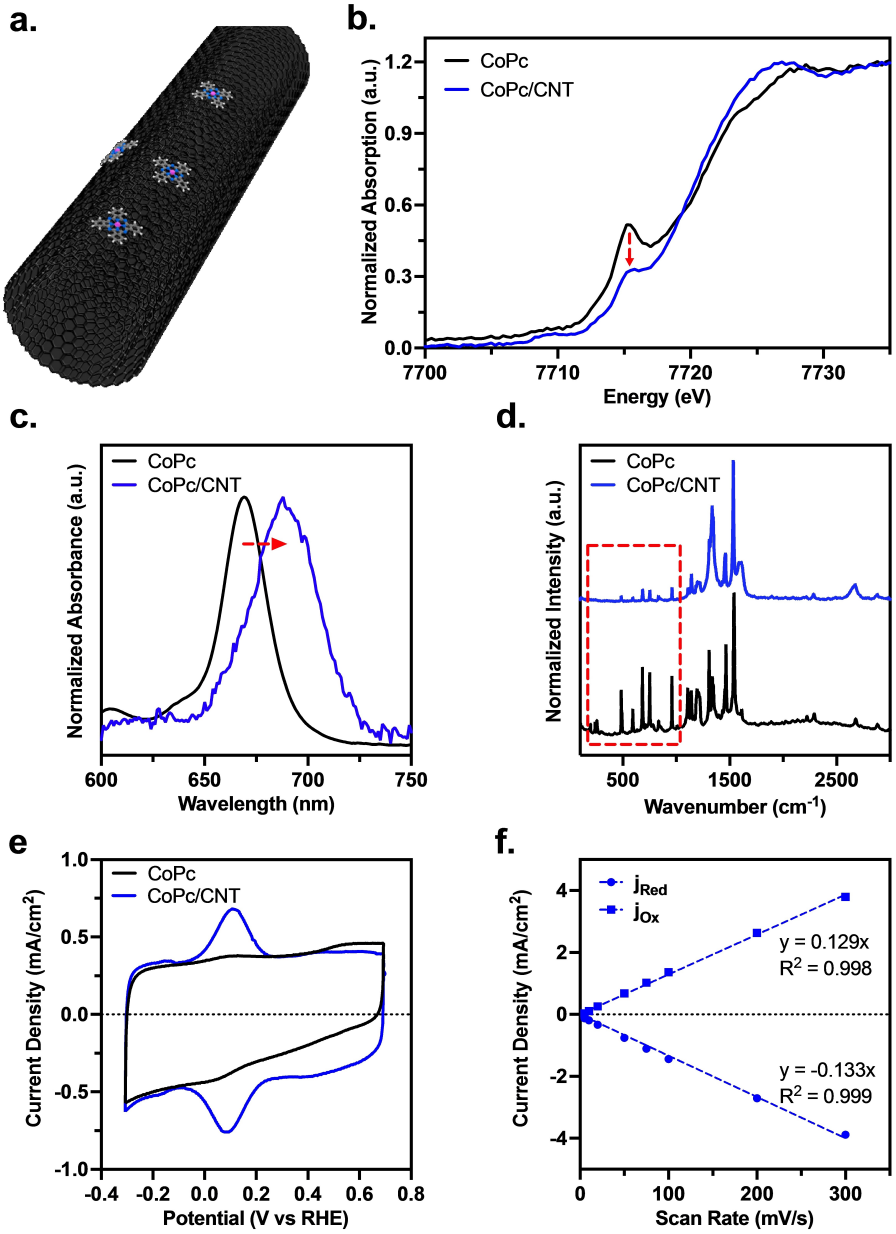

Figure 1. a. Schematic depiction of CoPc/CNT. b. Ex situ Co K-edge XANES of CoPc and CoPc/CNT. c. Normalized UV/Vis absorption of dissolved CoPc and dispersed CoPc/CNT in ethylene glycol. d. Raman spectra of CoPc and CoPc/CNT solids. e. CVs of CoPc and CoPc/CNT at 50 mV/s in Ar-saturated 0.1 M aqueous $KHCO_3$. f. Peak current density as a function of scan rate from CVs of CoPc/CNT.

In this work, we carried out X-ray absorption spectroscopy (XAS) studies, both ex situ and in situ, in combination with mechanistic electrocatalytic studies to answer these questions. We show that the CoPc/CNT catalyst contains a majority of monodispersed CoPc molecules with strong electronic coupling to the underlying graphitic CNT surface that causes a distortion from square planar molecular symmetry. By investigating the relationship between catalyst loading and FE_{MeOH} as well as that between j_{CO} and j_{MeOH}, we unveil an unusual property of the catalyst: CO is a highly labile intermediate that desorbs off the active site leading to competition between CO_2 and CO reduction. Comparing the electrocatalytic activity of three different CoPc-related compounds reveals that the bridging aza-N atoms are necessary to unlock the MeOH pathway. In situ X-ray absorption near edge structure (XANES) results verify that the resting state of the catalyst is Co(I) at all catalytically active potentials, and the molecule becomes increasingly non-centrosymmetric with negative applied potential possibly due to binding of the CO intermediate. Extended X-ray absorption fine structure (EXAFS) fitting indicates the $Co–N_4$ coordination remains intact throughout catalysis while a Co–C bond appears at catalytically active potentials.

Our previous characterization of CoPc/CNT has revealed molecular dispersion of CoPc on the graphitic CNT surface (Figure 1a), which is critical to the high catalytic performance towards CO_2 reduction to MeOH.[7,8d,15b,19] In this work, we further demonstrate that this interaction modifies the electronic and geometric structures of the CoPc molecule. Ex situ Co K-edge XAS shows a significant decrease in the intensity of the 7715 eV pre-edge feature upon molecular dispersion of CoPc onto CNTs (Figure 1b). The 7715 eV feature is assigned to the $1s \rightarrow 4p_z$ transition and is characteristic of square planar complexes.[20] It is well documented that axial coordination to create a square pyramidal complex will suppress this peak.[15a,21] The partial quenching of the feature indicates electron donation from the CNT into the Co $3d_z^2/4p_z$ orbitals of CoPc, thereby changing the molecular symmetry from D_{4h} to C_{4v}.[22] This electronic donation interaction is also evidenced by a red-shift in the UV/Vis absorption Q-band (Figures 1c, S1), which is known to occur when the electron density at the Co center of CoPc is increased, for example, by axial coordination of pyridine,[23] appending electron-donating groups to the Pc ligand,[7] or one-electron reduction of the molecule.[24] The electron donation from the CNT may make CoPc more nucleophilic by increasing the energy of the d_z^2 molecular orbital, and thus increase its reactivity towards CO_2 and even CO. Molecular dispersion of CoPc on the CNT surface is consistent with the suppression of Raman features under 1000 cm^{-1} (Figure 1d), possibly due to the limited out-of-plane vibrational modes of noncovalently anchored CoPc.[25] The highly symmetric cyclic voltammogram (CV) with small peak-to-peak separation is characteristic of fast electron transfer kinetics consistent with a surface-adsorbed catalyst (Figures 1e, f, and S2).[26] Much larger Co(II)/Co(I) redox waves in CoPc/CNT compared to free CoPc deposited on carbon paper, despite both catalysts having the same mass loading of CoPc molecules, clearly demonstrates that molecular dispersion on CNTs leads to a much larger fraction of electroactive molecules (61 % vs 3 %). Although these results help us understand the active sites of CoPc/CNT, they cannot fully decouple the role of the support interaction from the intrinsic activity of the CoPc molecule for catalytic CO_2 reduction to MeOH. Distinguishing these two factors is challenging due to the propensity of CoPc to form insulating aggregates in the solid state.

To better understand the role of CO in the CO_2-to-MeOH reaction pathway, we prepared electrodes with varied loadings of electrocatalyst and assessed their MeOH activity via controlled potential electrolysis (CPE) at two distinct potentials. In this study, we used $CoPc–NH_2$/CNT, which we previously demonstrated to display very similar catalytic activity to CoPc/CNT but with enhanced stability.[7] When plotting catalyst loading against FE_{MeOH} we observe an unexpected positive relationship (Figure 2a). At −0.9 V, the lowest-loading electrode (0.02 mg/cm^2) showed an FE_{MeOH} of 2 %, whereas the highest-loading electrode (0.8 mg/cm^2) achieved a much higher FE_{MeOH} of 28 %. What causes this massive discrepancy in selectivity? Plotting j_{MeOH} against j_{CO} helps us answer this question (Figure 2b). At −0.9 V, low j_{MeOH} is achieved at j_{CO} less than ≈17 mA/cm^2; however, once this threshold is reached, j_{MeOH} increases rapidly. A similar trend is observed at −1.0 V but the j_{CO} threshold is approximately half as large, possibly due to stronger CO binding at more negative applied potential. These data paint a picture of a labile CO-bound intermediate in the CO_2-to-MeOH reaction catalyzed by $CoPc–NH_2$ (Figure 2c): a high local concentration of CO needs to be generated in the catalyst microenvironment to push the reaction pathway to MeOH. The dependence of MeOH activity on the local CO concentration is further illustrated by a simple experiment using the $CoPc–NH_2$/CNT electrocatalyst with and without stirring the electrolyte in the cathode chamber. Without stirring, the catalyst yields 35 % FE_{MeOH}, whereas with vigorous stirring nearly all the MeOH activity is suppressed and replaced by selective CO production (Figure S3). This dependence helps explain why some other studies of CoPc electrocatalysts operating at lower current densities or under different mass transport conditions were not able to generate MeOH in significant yield. These results indicate that opportunities exist to improve the electrocatalytic performance of this system by modifying CoPc-based catalysts to increase the binding strength to CO or operate under high CO concentration.[10]

We next sought to identify the structural motifs present in CoPc and its peripherally substituted derivatives which activate them for CO_2 reduction to MeOH. To do this, we prepared and tested CNT-supported cobalt tetrabenzoporphyrin (CoTBP/CNT) and cobalt tetra-*tert*-butyl tetraazaporphyrin (CoTAP/CNT), which are structurally very similar to CoPc/CNT but missing certain functionalities (Figure 3a–d). CoTBP has C atoms in the place of the Pc ring's bridging aza-N atoms, while CoTAP has *t*Bu groups in the place of the Pc benzene rings. These two electrocatalysts were evaluated by CPE at several applied potentials and compared to CoPc/CNT and $CoPc–NH_2$/CNT (Figure S4). CoPc/CNT generates MeOH at all potentials from −0.8 to

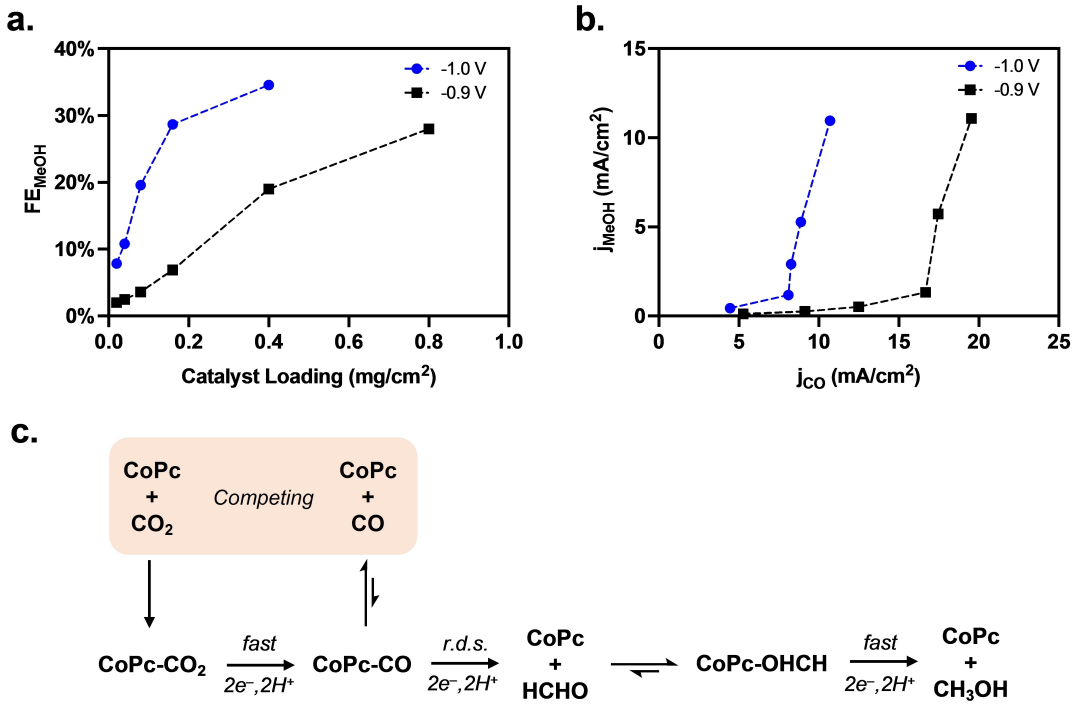

Figure 2. a. FE_{MeOH} as a function of CoPc–NH_2/CNT mass loading on the electrode during controlled potential electrolysis in CO_2-saturated 0.1 M aqueous $KHCO_3$. b. Dependence of j_{MeOH} on j_{CO}. c. Proposed reaction Scheme demonstrating the competing CO_2 and CO reduction reactions.

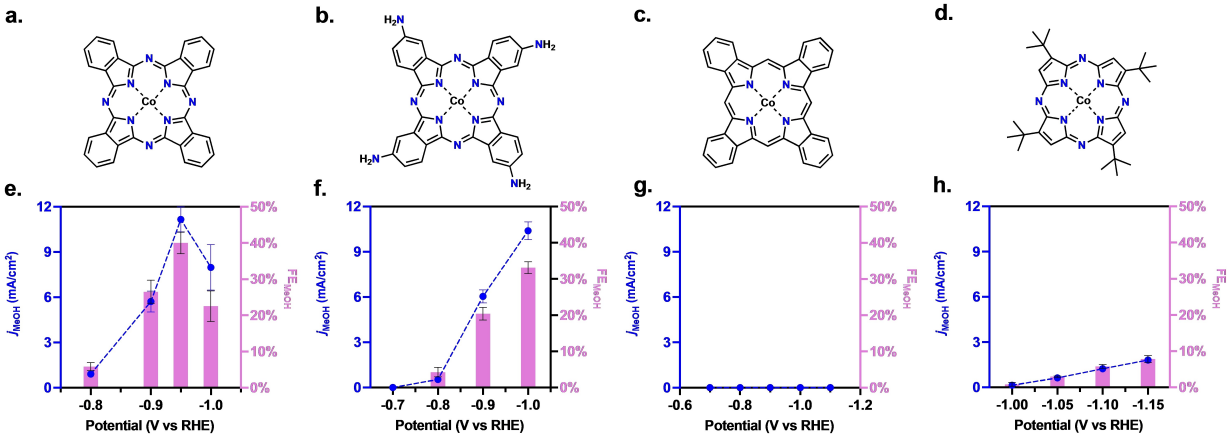

Figure 3. Molecular structures of a. CoPc, b. CoPc–NH_2, c. CoTBP, and d. CoTAP. Potential-dependent j_{MeOH} and FE_{MeOH} from electrochemical CO_2 reduction in 0.1 M aqueous $KHCO_3$ catalyzed by e. CoPc, f. CoPc–NH_2, g. CoTBP, and h. CoTAP molecules supported on CNTs.

−1.0 V with optimal selectivity above 40 % FE at −0.95 V (Figure 3e). CoPc–NH_2/CNT shows similar catalytic activity but with a slightly more negative optimal potential and lower max FE_{MeOH} (Figure 3f). In contrast, CoTBP/CNT does not generate MeOH at any of the tested applied potentials (Figure 3g). CoTAP/CNT shows some activity for CO_2 reduction to MeOH, although at even more negative potentials than CoPc–NH_2/CNT (Figure 3h). CoTAP/CNT achieves a FE_{MeOH} of 8 % and j_{MeOH} of 1.8 mA/cm^2 at −1.15 V. These results demonstrate that the bridging aza-N atoms in the Pc macrocycle are essential in creating the active site for MeOH production. This result helps explain why some other Co–N_4 electrocatalysts that are active for CO_2 reduction to CO, such as cobalt porphyrins, do not produce MeOH. The presence of bridging N atoms may either directly or indirectly influence the catalysis. For example, they may directly interact with reaction intermediates, they may operate as a proton relay (a theoretical study indicates that these N atoms get spontaneously hydrogenated at MeOH producing potentials),[15c] or they may alter the binding strength of Co to CO. These results illustrate the role of second-shell coordination effects in single atom catalysts, and the underlying opportunity to tailor active sites via mechanism-guided optimization.

To better understand the active site for MeOH production, we studied CoPc–NH_2/CNT under electrocatalytic CO_2

reduction conditions by in situ XAS with a custom-designed cell for fluorescence detection (Figures S5 and S6). It is important to note that CoPc–NH_2/CNT is stable for 12+ hours under CO_2-to-MeOH conditions whereas CoPc/CNT deactivates in a few hours; therefore, multiple-hours long measurements such as in situ XAS studies should utilize the CoPc–NH_2/CNT catalyst to ensure they are probing the reaction of interest. At open circuit voltage (OCV), there are two distinct pre-edge features at 7710 eV and 7715 eV (Figure 4a). Upon application of a mildly cathodic potential of −0.3 V, which is past the first reduction of CoPc–NH_2 (observed at ≈0.0 V in the CV in Figure S7) but before the onset of catalytic current, we see a significant edge shift of the XANES spectra (Figure 4b). This is strong evidence for the first reduction of CoPc–NH_2 being metal-based Co(II)→Co(I), which might have been incorrectly assigned in our earlier work.[3a] Note that this reduction is not adequate for CoPc–NH_2 to reduce CO_2 and further reductions are needed

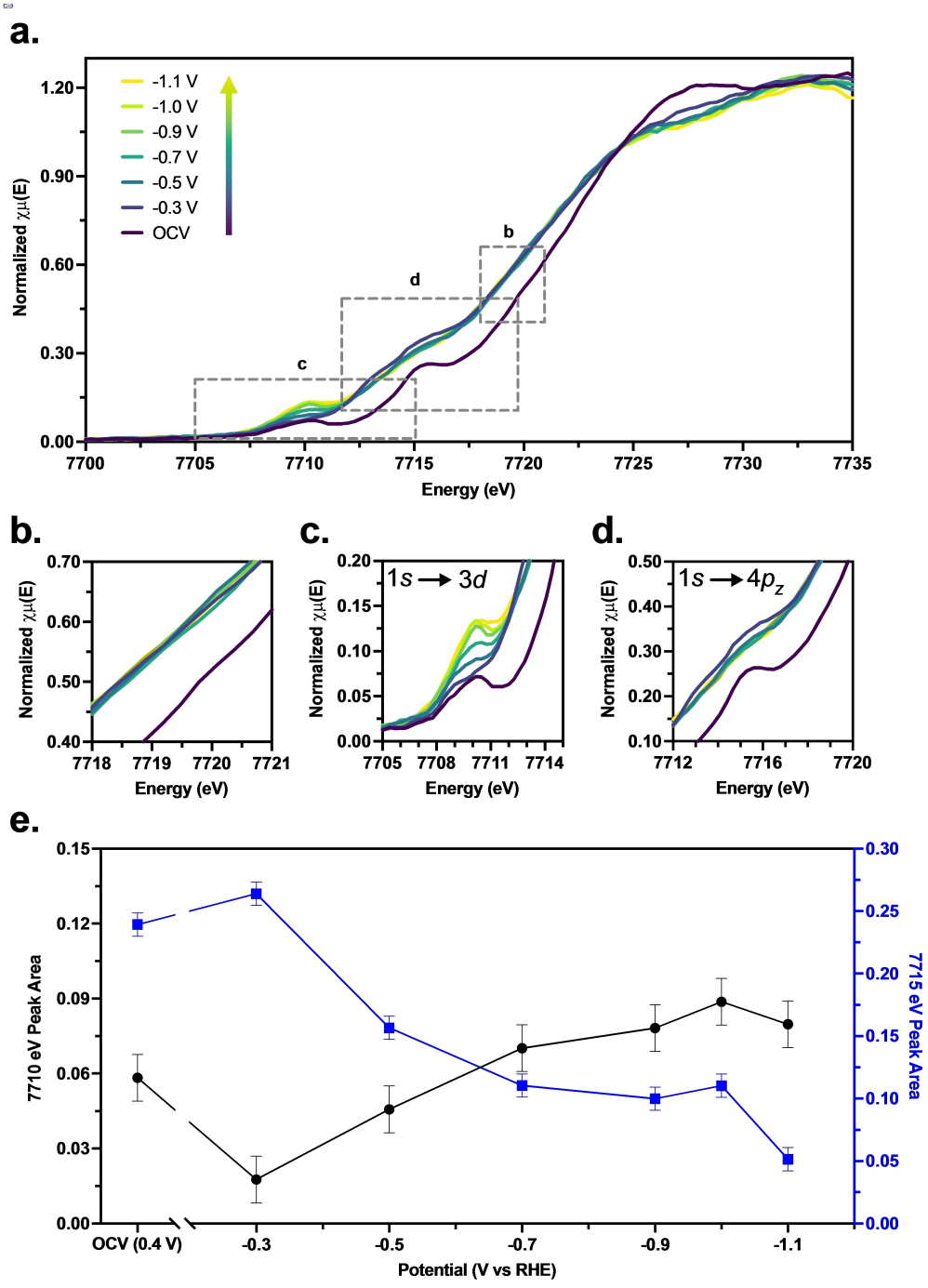

Figure 4. a. Co K-edge XANES spectra of CoPc–NH_2/CNT at varied applied potential in CO_2-saturated 0.1 M aqueous $KHCO_3$. b. Zoom in on edge shift. c. Zoom in on 7710 eV feature. d. Zoom in on 7715 eV feature. e. Pre-edge peak areas (Figure S9) as a function of applied potential.

to activate the catalyst.[27] As the potential is stepped up more negatively all the way up to −1.1 V, the edge position does not move, indicating that the second reduction is ligand-based and the Co(I) oxidation state persists. The shift in edge position is mostly reversible upon returning to the original OCV potential (Figure S8). The pre-edge feature at 7710 eV is assigned to the Co 1s→3d transition. Upon first reduction of the CoPc–NH_2 molecule (going from OCV to −0.3 V), the peak is almost completely quenched (Figures 4c, e and S9), which is likely due to the increased density of states in the Co 3d orbitals from an electron being added into the $3d_z^2$ orbital. As the applied potential is shifted more negative, the pre-edge feature increases in area before beginning to level off between −0.9 V and −1.1 V, the optimal potential range for MeOH production. Considering that this feature is known to increase in intensity as a metal site distorts from centrosymmetric to a non-centrosymmetric coordination environment, a result of increased 3d+4p mixing in the reduced symmetry environment,[15a,22] we correlate its increase to the axial binding of the CO intermediate to the Co center. As noted previously, the pre-edge feature at 7715 eV is assigned to the 1 s→$4p_z$ transition, which is known to be sensitive to axial coordination. Upon the first reduction from OCV to −0.3 V, there is no significant change to the peak area, although the peak has visibly broadened (Figure 4d, e). Upon applying more negative potentials, the peak decreases and virtually disappears. The potential-dependent decrease of the 7715 eV pre-edge peak matches closely to the catalytic onset of CO_2 reduction (Figure S10), reflecting a coordination change caused by axial binding of CO_2 or CO to the Co center in the reduction intermediates.

EXAFS fitting of the in situ XAS results reveals that Co–N_4 coordination is maintained at all applied potentials while Co–C coordination appears at catalytically active potentials (Figure 5a–c, Table S1). R-space fitting results show Co–N coordination at a bond length of 1.92 Å. Co–C coordination appears at a bond length of 1.79 Å at −0.7 V and −1.1 V, potentials where CoPc–NH_2/CNT is catalytically active for CO_2 reduction to CO and MeOH, respectively. These results demonstrate that the molecular structure of CoPc–NH_2 is maintained throughout electrocatalysis. Considering that the Co–C coordination appears in the active potential range of CO_2 reduction to CO and then to MeOH, we hypothesize that the resting state of the CoPc–NH_2 electrocatalyst may be five-coordinate with axially bound CO (Figure 5d). The Co–C bond length from our EXAFS fitting matches well with the bond length of a $Co(I)Pc^{1-}$–CO intermediate predicted in a prior computational study.[15c] The presence of bound CO on the active site under working conditions agrees well with the in situ XANES results discussed above and is consistent with the finding that proton-coupled electron transfer to the CO

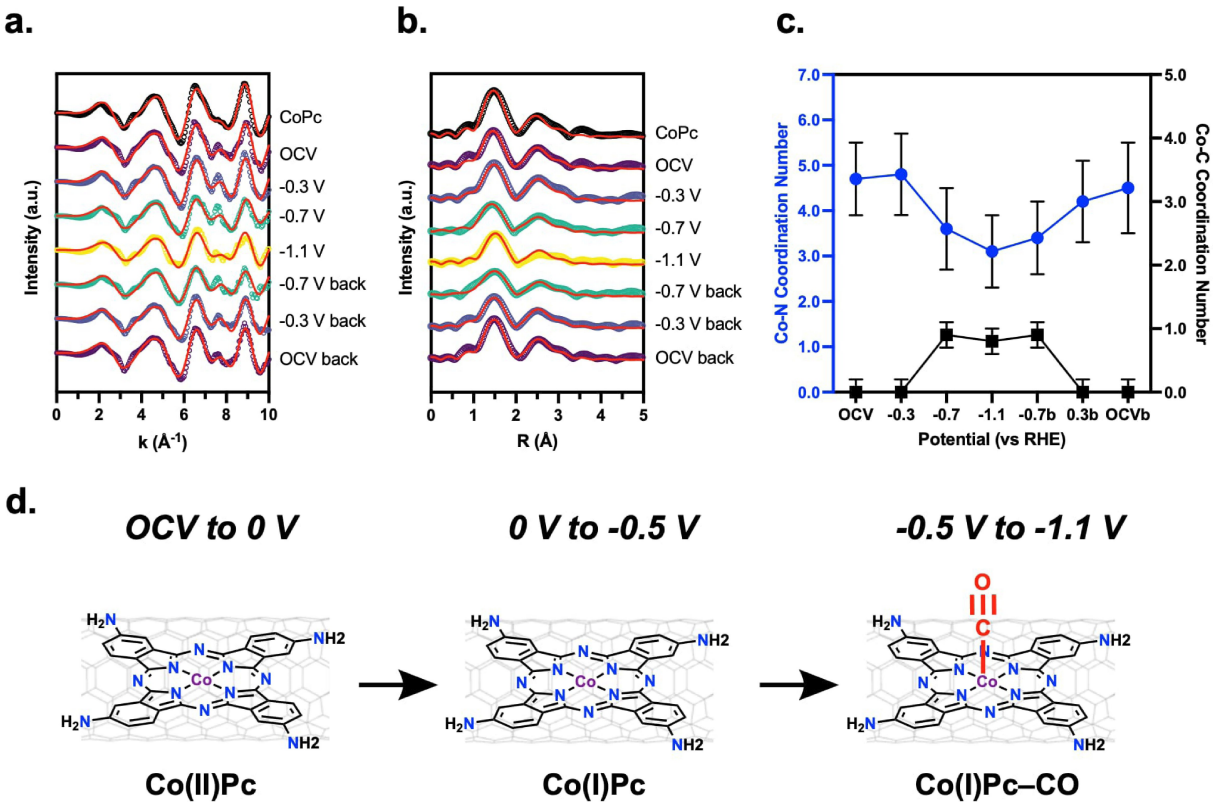

Figure 5. a. k-space EXAFS results and fitting from in situ XAS of CoPc–NH_2/CNT during electrochemical CO_2 reduction. b. R-space EXAFS results and fitting. **c**. Coordination number for Co–N and Co–C bonds as a function of applied potential. **d**. Structure models of resting state CoPc–NH_2/CNT within different applied potential windows.

intermediate is the rate-determining step of the CO_2-to-MeOH reaction.[7,10]

In summary, our spectroscopic and electrocatalytic investigations advances the field's mechanistic understanding of electrochemical CO_2 reduction to MeOH on CoPc-based electrocatalysts. Molecular level dispersion of CoPc on the CNT support is key to the high catalytic activity. CO is a labile intermediate that must be produced with high enough local concentration in order to be further reduced to MeOH. The bridging aza-N atoms in the Pc structure are critical for CoPc's activity to form MeOH from CO_2 reduction. Oxidation state and coordination environment changes of the Co center under reaction conditions, as revealed by in situ XAS measurements, are necessary to propel the CO_2-to-MeOH conversion. These results open the door for further work to improve the electrocatalytic performance of this system, as well as push forward the development of other molecular electrocatalysts for multi-electron CO_2 reduction.

Acknowledgements

This work was supported by U.S. National Science Foundation, grant numbers CBET-2129963 (molecule-nanotube interaction research) and CHE-1651717 (in situ XAS work, C.L.R. and H.W.). Z.F. acknowledges support from U.S. National Science Foundation, grant number CBET-2151049, for in situ XAS work. The CoTBP synthesis work (G.H. and G.W.B.) was supported by U.S. Department of Energy, Chemical Sciences, Geosciences, and Biosciences Division, Office of Basic Energy Sciences, Office of Science, grant number DEFG02-07ER15909, and a generous donation from the TomKat Charitable Trust.

Conflict of Interest

The authors declare no conflict of interest.

Data Availability Statement

The data that support the findings of this study are available from the corresponding author upon reasonable request.

Keywords: CO_2 Reduction · Electrocatalysis · In Situ Characterization · Molecular Catalyst · X-Ray Absorption Spectroscopy

[1] a) Q. Feng, Y. Sun, X. Gu, Z. Dong, *Electrocatalysis* **2022**, *13*, 675–690; b) Y. Wu, Y. Liang, H. Wang, *Acc. Chem. Res.* **2021**, *54*, 3149–3159.

[2] C. M. Lieber, N. S. Lewis, *J. Am. Chem. Soc.* **1984**, *106*, 5033–5034.

[3] a) X. Zhang, Z. Wu, X. Zhang, L. Li, Y. Li, H. Xu, X. Li, X. Yu, Z. Zhang, Y. Liang, H. Wang, *Nat. Commun.* **2017**, *8*, 14675; b) M. Wang, K. Torbensen, D. Salvatore, S. Ren, D. Joulié, F. Dumoulin, D. Mendoza, B. Lassalle-Kaiser, U. Işci, C. P. Berlinguette, M. Robert, *Nat. Commun.* **2019**, *10*, 3602; c) L. Xiong, X. Fu, Y. Zhou, P. Nian, Z. Wang, Q. Yue, *ACS Catal.* **2023**, *13*, 6652–6660; d) X. Wu, J. W. Sun, P. F. Liu, J. Y. Zhao, Y. Liu, L. Guo, S. Dai, H. G. Yang, H. Zhao, *Adv. Funct. Mater.* **2022**, *32*, 2107301.

[4] T. L. Soucy, Y. Liu, J. B. Eisenberg, C. C. L. McCrory, *ACS Appl. Energ. Mater.* **2022**, *5*, 159–169.

[5] a) R. Matheu, E. Gutierrez-Puebla, M. Á. Monge, C. S. Diercks, J. Kang, M. S. Prévot, X. Pei, N. Hanikel, B. Zhang, P. Yang, O. M. Yaghi, *J. Am. Chem. Soc.* **2019**, *141*, 17081–17085; b) H. Wu, M. Zeng, X. Zhu, C. Tian, B. Mei, Y. Song, X.-L. Du, Z. Jiang, L. He, C. Xia, S. Dai, *ChemElectroChem* **2018**, *5*, 2717–2721.

[6] S. Kapusta, N. Hackerman, *J. Electrochem. Soc.* **1984**, *131*, 1511–1514.

[7] Y. Wu, Z. Jiang, X. Lu, Y. Liang, H. Wang, *Nature* **2019**, *575*, 639–642.

[8] a) Y. Wu, G. Hu, C. L. Rooney, G. W. Brudvig, H. Wang, *ChemSusChem* **2020**, *13*, 6296; b) Y. Wu, Z. Jiang, Z. Lin, Y. Liang, H. Wang, *Nat. Sustainability* **2021**, *4*, 725–730; c) C. L. Rooney, Y. Wu, Z. Tao, H. Wang, *J. Am. Chem. Soc.* **2021**, *143*, 19983–19991; d) B. Shang, C. L. Rooney, D. J. Gallagher, B. T. Wang, A. Krayev, H. Shema, O. Leitner, N. J. Harmon, L. Xiao, C. Sheehan, S. R. Bottum, E. Gross, J. F. Cahoon, T. E. Mallouk, H. Wang, *Angew. Chem. Int. Ed.* **2023**, *62*, e202215213.

[9] J. Su, C. B. Musgrave, Y. Song, L. Huang, Y. Liu, G. Li, Y. Xin, P. Xiong, M. M.-J. Li, H. Wu, M. Zhu, H. M. Chen, J. Zhang, H. Shen, B. Z. Tang, M. Robert, W. A. Goddard, R. Ye, *Nat. Catal.* **2023**, https://doi.org/10.1038/s41929–023–01005–3.

[10] J. Li, B. Shang, Y. Gao, S. Cheon, C. L. Rooney, H. Wang, *Nat. Synth.* **2023**, https://doi.org/10.1038/s44160–023–00384–6.

[11] a) X.-M. Hu, M. H. Rønne, S. U. Pedersen, T. Skrydstrup, K. Daasbjerg, *Angew. Chem. Int. Ed.* **2017**, *56*, 6468–6472; b) G. F. Manbeck, E. Fujita, *J. Porphyrins Phthalocyanines* **2015**, *19*, 45–64.

[12] J. Grodkowski, P. Neta, E. Fujita, A. Mahammed, L. Simkhovich, Z. Gross, *J. Phys. Chem. A* **2002**, *106*, 4772–4778.

[13] P. Hou, W. Song, X. Wang, Z. Hu, P. Kang, *Small* **2020**, *16*, 2001896.

[14] E. Boutin, M. Wang, J. C. Lin, M. Mesnage, D. Mendoza, B. Lassalle-Kaiser, C. Hahn, T. F. Jaramillo, M. Robert, *Angew. Chem. Int. Ed.* **2019**, *58*, 16172–16176.

[15] a) Y. Liu, A. Deb, K. Y. Leung, W. Nie, W. S. Dean, J. E. Penner-Hahn, C. C. L. McCrory, *Dalton Trans.* **2020**, *49*, 16329–16339; b) X. Chen, D. Wei, M. S. G. Ahlquist, *Organometallics* **2021**, *40*, 3087–3093; c) L.-L. Shi, M. Li, B. You, R.-Z. Liao, *Inorg. Chem.* **2022**, *61*, 16549–16564.

[16] a) M. Zhu, R. Ye, K. Jin, N. Lazouski, K. Manthiram, *ACS Energy Lett.* **2018**, *3*, 1381–1386; b) M. Mahmood, D. Masheder, C. Harty, *J. Appl. Electrochem.* **1987**, *17*, 1223–1227.

[17] a) Q. Chang, Y. Liu, J.-H. Lee, D. Ologunagba, S. Hwang, Z. Xie, S. Kattel, J. H. Lee, J. G. Chen, *J. Am. Chem. Soc.* **2022**, *144*, 16131–16138; b) Z. Zhang, J. Xiao, X.-J. Chen, S. Yu, L. Yu, R. Si, Y. Wang, S. Wang, X. Meng, Y. Wang, Z.-Q. Tian, D. Deng, *Angew. Chem. Int. Ed.* **2018**, *57*, 16339–16342; c) H. Li, J. Wei, X. Zhu, L. Gan, T. Cheng, J. Li, *J. Phys. Chem. C* **2022**, *126*, 9665–9672; d) S. Vijay, W. Ju, S. Brückner, S.-C. Tsang, P. Strasser, K. Chan, *Nat. Catal.* **2021**, *4*, 1024–1031.

[18] X. Ren, J. Zhao, X. Li, J. Shao, B. Pan, A. Salamé, E. Boutin, T. Groizard, S. Wang, J. Ding, X. Zhang, W.-Y. Huang, W.-J. Zeng, C. Liu, Y. Li, S.-F. Hung, Y. Huang, M. Robert, B. Liu, *Nat. Commun.* **2023**, *14*, 3401.

[19] C. Choi, X. Wang, S. Kwon, J. L. Hart, C. L. Rooney, N. J. Harmon, Q. P. Sam, J. J. Cha, W. A. Goddard, M. Elimelech, H. Wang, *Nat. Nanotechnol.* **2023**, *18*, 160–167.
[20] F. B. J. H. Zagal, J.-P. Dodelet, *N4-Macrocyclic Metal Complexes*, *Vol. 1*, Springer, New York, NY, **2006**.
[21] N. Li, W. Lu, K. Pei, W. Chen, *RSC Adv.* **2015**, *5*, 9374–9380.
[22] J. C. Swarbrick, T.-C. Weng, K. Schulte, A. N. Khlobystov, P. Glatzel, *Phys. Chem. Chem. Phys.* **2010**, *12*, 9693.
[23] K. E. Rivera Cruz, Y. Liu, T. L. Soucy, P. M. Zimmerman, C. C. L. McCrory, *ACS Catal.* **2021**, *11*, 13203–13216.
[24] T. T. Tasso, T. Furuyama, N. Kobayashi, *Inorg. Chem.* **2013**, *52*, 9206–9215.
[25] D. Nguyen, G. Kang, N. Chiang, X. Chen, T. Seideman, M. C. Hersam, G. C. Schatz, R. P. Van Duyne, *J. Am. Chem. Soc.* **2018**, *140*, 5948–5954.
[26] N. Elgrishi, K. J. Rountree, B. D. McCarthy, E. S. Rountree, T. T. Eisenhart, J. L. Dempsey, *J. Chem. Educ.* **2018**, *95*, 197–206.
[27] a) C. Choi, F. Zhao, J. L. Hart, Y. Gao, F. Menges, C. L. Rooney, N. J. Harmon, B. Shang, Z. Xu, S. Suo, Q. Sam, J. J. Cha, T. Lian, H. Wang, *Angew. Chem. Int. Ed.* **2023**, *62*, e202302152; b) B. Shang, F. Zhao, C. Choi, X. Jia, M. Pauly, Y. Wu, Z. Tao, Y. Zhong, N. Harmon, P. A. Maggard, T. Lian, N. Hazari, H. Wang, *ACS Energy Lett.* **2022**, *7*, 2265–2272.

Manuscript received: July 25, 2023
Accepted manuscript online: October 11, 2023
Version of record online: December 1, 2023